Modeling of a plasma column produced and sustained by a traveling electromagnetic wave in the presence of a constant axial magnetic field

E. Benova
Department of Physics, Institute for Foreign Students, BG-1111 Sofia, Bulgaria

I. Zhelyazkov* and P. Staikov
Faculty of Physics, Sofia University, BG-1126 Sofia, Bulgaria

F. Cap
Institut für Theoretische Physik, Universität Innsbruck, A-6020 Innsbruck, Austria
(Received 17 August 1990; revised manuscript received 31 January 1991)

We present the basic equations for modeling a plasma column produced and sustained by a traveling electromagnetic wave in the presence of a constant external magnetic field. The model consists of two equations—a local-dispersion relationship and a wave-energy-balance equation—and a relation between the absorbed wave power per unit length averaged across the column (proportional to the squared-wave electric field) and the local electron number density. The dispersion relation and the balance equation are derived in explicit forms and depend on two numerical parameters $\sigma=\omega R/c$ (ω being the wave angular frequency, R the plasma column radius, c speed of light) and $\Omega=\omega_c/\omega$ (ω_c is the electron cyclotron frequency). The limit of an infinite external magnetic field ($\Omega\rightarrow\infty$) is also considered. The influence of the two parameters Ω and σ on the dimensionless axial profiles of the wave characteristics and plasma column density, obtained by numerical solution of the basic equations, has been studied for two different gas-discharge regimes. A three-dimensional wave structure has been obtained, and it is shown that the wave can be a generalized surface mode, a pure surface, or a pseudosurface one. The results obtained are in agreement with the available experimental data.

I. INTRODUCTION

In recent years, increasing interest has been shown in the study of rf and microwave discharges produced and sustained by traveling electromagnetic waves. Due to their stability and good reproducibility over a large pressure range, such discharges have found many applications in various fields of technology and research [1–4]. Up to now, these discharges have been extensively studied mainly for isotropic plasmas, for various operating conditions, namely gas nature [2–10], pressure [7,8,10,11], plasma radius [7,12,13], and wave frequency [12]. The rf or microwave power, supplied by a high-frequency generator, is coupled to the discharge through a matched structure (sometimes referred to as surfatron [14], surfaguide [15], waveguide surfatron [16], or Ro-box [17]), and is carried by an electromagnetic wave simultaneously propagating and ionizing the gas. Note that the physics of the phenomenon is the same for all these wave exciters. In fact, the electric field of the wave heats the electrons that ionize the gas, ensuring in this way further wave propagation. The wave power axially decreases from the gap of the exciter to the end of the plasma column, due to energy transfer of the high-frequency field to the electrons. Thus, the electron number density also decreases along the column.

It is natural to expect that a constant external magnetic field should visibly change the conditions for plasma column production, as well as the structure of the column itself. First, in a magnetic field, the plasma becomes anisotropic, which reflects in a change of the propagation characteristics and field structure of the electromagnetic wave. Second, a relatively strong axial magnetic field must reduce the radial electron diffusion, which leads to a decrease of the axial plasma density gradient and the electron temperature, too. There are few experimental results concerning the influence of the magnetic field on an electromagnetic-wave-sustained plasma column. Moisan *et al.* [18] state, from experiment, that a constant axial magnetic field facilitates plasma production. In another work by Moisan, Pantel and Ricard [19], the effect of such a magnetic field on the density radial distributions of excited atoms (in radiative and metastable states) has been studied experimentally. Recently, Pasquiers *et al.* [20,21] reported on an experimental investigation of a low-pressure argon discharge produced by an electromagnetic wave with an external magnetic field. Anghelova *et al.* [22] have examined experimentally the axial profiles of the plasma parameters (electron temperature T_e and the electron number density n) of a helium low-pressure gas-discharge column sustained by a traveling electromagnetic wave in the presence of a magnetic field. It is found that the electron temperature is diminished and the plasma density is increased (accompanied by a decrease of its axial gradient) in comparison with the magnitudes of the same parameters and characteristics of an isotropic plasma column.

The modeling of a plasma column produced and sustained by a traveling electromagnetic wave is a challenging task. Most of the observed axial structures of low-pressure gas discharges in the absence of a magnetic field are adequately described by the existing theories (Glaude *et al.* [5] Mateev, Zhelyazkov, and Atanassov [23], Zakrzewski [24], Ferreira [25,26], Zhelyazkov, Benova, and Atanassov [27], Zhelyazkov, Atanassov, and Benova [28], Boisse-Laporte *et al.* [8] Sá and Ferreira [29], Zhe-

lyazakov and Benova [30], and Benova and Zhelyazkov [31]) assuming that the sustaining electromagnetic wave is an azimuthally symmetric surface TM mode. A theoretical model of a plasma column produced by a guided electrostatic wave in the presence of a constant axial magnetic field B_0 (Zhelyazkov, Benova, and Atanassov [32]) shows that a significant influence of the magnetic field on the properties of the plasma column occurs only when the angular wave frequency ω is lower than the electron cyclotron frequency ω_c ($=eB_0/mc$), that is, when $\omega_c/\omega \equiv \Omega > 1$. The magnetic field (called a "strong magnetic field" as $\Omega > 1$) modifies the wave-field structure (in the electrostatic limit the wave becomes a pseudosurface [33] mode) and decreases the axial plasma density gradient. Moreover, it is predicted that for a given high-frequency power emerging from the wave launcher, the column length should increase with increasing Ω, i.e., the stronger the magnetic field, the longer the column length. The characteristics of the plasma column should depend also on the gas-discharge regime (a diffusion or recombination one), specified by the gas pressure, the tube diameter, and elementary processes in the ionized medium. Recently, Pasquiers *et al.* [34] presented an experimental investigation on the action of a static magnetic field on an argon discharge produced by a traveling wave. Their paper includes also some theoretical modeling based on an electromagnetic treatment of the problem. Both their experimental and theoretical results generally confirm the main conclusions of Refs. [22] and [32], pointing out, however, the narrow range of applicability of the simplest model [32] (at low electron number densities and low microwave frequencies).

It is the purpose of this paper to present a general model of the axial structure of a plasma column sustained by an electromagnetic wave in the presence of an external constant axial magnetic field, as well as the axial profiles of all wave characteristics (wave number, wave power, electric and magnetic wave-field components). If the theoretical modeling of Pasquiers *et al.* [34] considers only a particular experimental setup (given plasma radius, wave frequency, gas pressure and magnetic-field ranges) assuming occurrence of diffusion gas-discharge conditions, we study the dependence of the discharge anatomy and wave characteristics on dimensionless parameters calculated on the basis of different plasma radii R, wave frequencies ω, external magnetic-field inductions B_0, and gas-discharge regimes (free fall or diffusion and recombination ones). Moreover, we examine the limiting case of an infinite external magnetic field ($B_0 \to \infty$), as well as the possibility of creating plasma columns by means of "zone-depending" electromagnetic wave modes when the magnetic field is strong enough ($\Omega > 1$). The latter directly follows from the possibility for multivalued solutions to the wave dispersion relation [32].

It has been shown in Ref. [27] that the axial structure of a plasma column produced by an electromagnetic surface wave under the assumptions for weakly collisional plasma ($\nu \ll \omega$, ν being the collision frequency for momentum transfer) and slow axial variations of the electron number density, the wave number, and the wave-field components is specified by an equation connecting the surface-wave dispersion characteristics and plasma column parameters [Eq. (9) there]. In the zeroth-order approximation with respect to all logarithmic derivatives on z contained in that equation, one obtains a local-dispersion relation, while the first-order approximation (9) gives an equation for the balance of the surface-wave energy in a column with weak longitudinal density inhomogeneity. The numerical solving of these two equations with additional assumptions (concerning the gas-discharge regime) specifying the relation between the squared-wave electric field $|\mathbf{E}|^2$ and the local electron number density n gives the axial structure of the column. The same results follow from the solving of independently derived dispersion and energy balance equations [35,28]. Further on, we will follow the concept used in Refs. [28] and [32]—it is more convenient and more instructive to derive a local-dispersion relation and solve it together with a wave-energy-balance equation assuming a suitable additional condition between $|\mathbf{E}|^2$ and n. As a result, one obtains "universal" axial profiles of dimensionless electron number density and all wave characteristics depending on three numerical parameters. In addition to our previous works, we give here the axial dependencies of all electromagnetic wave-field components as well as their radial distributions in order to compare the latter with similar figures plotted by Pasquiers *et al.* [34]. Finally, we apply our theoretical results to particular experimental data.

The organization of the paper is as follows. In Sec. II we present the formulation of the problem and the basic assumptions. Section III is devoted to the derivation of the dispersion relation and the wave-energy-balance equation. In Sec. IV we expose the numerical calculations and results, and in Sec. V give the comparison with the experiment. The paper ends with a discussion concerning the future improvement of the model.

II. FORMULATION OF THE PROBLEM AND BASIC ASSUMPTIONS

We consider a cylindrical plasma column of radius R sustained by a high-frequency azimuthally symmetric electromagnetic wave of angular frequency ω excited at the one side of the tube (Fig. 1). The plasma is immersed in a constant axial magnetic field $\mathbf{B}_0=(0,0,B_0)$. Since the wave frequency ω and electron cyclotron frequency ω_c are normally much higher than the ion plasma and ion cyclotron frequencies, further on we can neglect the ion dynamics. We assume that the electron number density is radially constant:

$$n = \bar{n} \equiv (2/R^2)\int_0^R dr\, r\, n(r) ,$$

but it may depend weakly on z. For simplicity, the electron-neutral collision tensor is considered to be isotropic, so we can use the usual collision frequency for momentum transfer ν. The electromagnetic wave propagates without any reflection along the plasma column, and the latter is assumed bounded by vacuum. At present we ignore the effect of the plasma container (a dielectric tube with given thickness and permittivity) and, say, a metal screen on the dispersion properties of the wave and on its energy outlay. The plasma anisotropy,

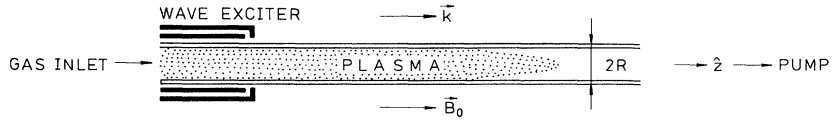

FIG. 1. Schematic view of an experimental situation.

caused by the external magnetic field $\mathbf{B}_0$, is taken into account by presenting the plasma permittivity in a tensor form:

$$\vec{\epsilon}^{\,p}=\begin{bmatrix} \tilde{\epsilon}_\perp & i\tilde{g} & 0 \\ -i\tilde{g} & \tilde{\epsilon}_\perp & 0 \\ 0 & 0 & \tilde{\epsilon}_\parallel \end{bmatrix}, \tag{1}$$

with

$$\tilde{\epsilon}_\perp=1-\omega_p^2(\omega+i\nu)/\omega[(\omega+i\nu)^2-\omega_c^2] ,$$

$$\tilde{\epsilon}_\parallel=1-\omega_p^2/\omega(\omega+i\nu) ,$$

$$\tilde{g}=\omega_p^2\omega_c/\omega[(\omega+i\nu)^2-\omega_c^2] .$$

Here $\omega_p=(4\pi ne^2/m)^{1/2}$ is the electron plasma frequency.

An essential feature of the problem is that we consider the plasma created as a weakly collisional one ($\nu \ll \omega$); moreover, the wave frequency ω is far enough from the electron cyclotron frequency ω_c. Then by neglecting the small terms of order ν^2/ω^2 or $\nu^2/(\omega^2-\omega_c^2)$, we have

$$\epsilon_\perp \equiv \mathrm{Re}(\tilde{\epsilon}_\perp)=1-\omega_p^2/(\omega^2-\omega_c^2)=1-N/(1-\Omega^2) ,$$

$$\epsilon_\parallel \equiv \mathrm{Re}(\tilde{\epsilon}_\parallel)=1-\omega_p^2/\omega^2=1-N ,$$

$$g \equiv \mathrm{Re}(\tilde{g})=\omega_p^2\omega_c/\omega(\omega^2-\omega_c^2)=N\Omega/(1-\Omega^2) ,$$

with $N=n/n_{cr}$ (n_{cr} being $m\omega^2/4\pi e^2$), $\Omega=\omega_c/\omega$, and

$$\mathrm{Im}(\tilde{\epsilon}_\perp)=(\nu/\omega)\omega_p^2(\omega^2+\omega_c^2)/(\omega^2-\omega_c^2)^2$$
$$=(\nu/\omega)N(1+\Omega^2)/(1-\Omega^2)^2 ,$$

$$\mathrm{Im}(\tilde{\epsilon}_\parallel)=(\nu/\omega)\omega_p^2/\omega^2=(\nu/\omega)N ,$$

$$\mathrm{Im}(\tilde{g})=-2\nu\omega_p^2\omega_c/(\omega^2-\omega_c^2)^2$$
$$=-2(\nu/\omega)N\Omega/(1-\Omega^2)^2 .$$

The propagation of the electromagnetic wave along the plasma column is governed by Maxwell's equations for both media (p, plasma; v, vacuum):

$$\nabla\times\mathbf{E}^{p,v}=-\frac{1}{c}\frac{\partial}{\partial t}\mathbf{B}^{p,v} ,$$

$$\nabla\times\mathbf{B}^{p,v}=\frac{1}{c}\frac{\partial}{\partial t}\mathbf{D}^{p,v} , \tag{2}$$

$$D=\vec{\epsilon}\cdot\mathbf{E} .$$

In (2) $\vec{\epsilon}^{\,p}$ is taken from (1) and $\vec{\epsilon}^{\,v}\equiv\underline{I}$, the unity matrix. The boundary conditions express the continuity of the axial and azimuthal components of the electromagnetic field at the plasma-vacuum interface ($r=R$):

$$\mathcal{E}_z^p|_{r=R}=\mathcal{E}_z^v|_{r=R},\quad \mathcal{B}_z^p|_{r=R}=\mathcal{B}_z^v|_{r=R} ,$$

and

$$\mathcal{E}_\varphi^p|_{r=R}=\mathcal{E}_\varphi^v|_{r=R},\quad \mathcal{B}_\varphi^p|_{r=R}=\mathcal{B}_\varphi^v|_{r=R} . \tag{3}$$

III. DISPERSION RELATION AND ENERGY-BALANCE EQUATION

In order to derive a dispersion relation and an energy-balance equation for high-frequency electromagnetic waves propagating along an axially inhomogeneous plasma column, immersed in an external magnetic field $\mathbf{B}_0$, we take the wave dependence on space and time in the form

$$\mathcal{E}_{r,\varphi,z}^{p,v}(r,z,t)=\mathrm{Re}\left[F_{r,\varphi,z}^{p,v}(r;z)\mathcal{E}(z)\times\exp\left[-i\omega t+i\int_{z_0}^{z}dz'k(z')\right]\right] ,$$

$$\mathcal{B}_{r,\varphi,z}^{p,v}(r,z,t)=\mathrm{Re}\left[G_{r,\varphi,z}^{p,v}(r;z)\mathcal{E}(z)\times\exp\left[-i\omega t+i\int_{z_0}^{z}dz'k(z')\right]\right] , \tag{4}$$

where k is the wave number, $F_{r,\varphi,z}(r;z)\mathcal{E}(z)$ and $G_{r,\varphi,z}(r;z)\mathcal{E}(z)$ are the wave electric- and magnetic-field amplitudes, respectively, which depend slowly on z [$H^{-1}(\partial H/\partial z)\ll k$, H being F, G, $\mathcal{E}$, k, or n]; the r dependence is specified by the governing equations (2). In (4), $\mathcal{E}(z)$ denotes $|\mathcal{E}_z^p(R,z)|$. We note that for either $B_0=0$ or infinite B_0, the electromagnetic wave is a TM mode ($B_z=0$), whereas for finite B_0 it is a hybrid mode ($\mathcal{B}_z\neq 0$ and $\mathcal{E}_z\neq 0$). It is straightforward by introducing the dimensionless variables $\rho\equiv r/R$, $x\equiv kR$, and the parameter $\sigma\equiv\omega R/c$ to obtain from Maxwell's equations (2) the following coupled equations for the dimensionless axial wave components into an ionized medium:

$$\frac{1}{\rho}\frac{\partial}{\partial\rho}\left[\rho\frac{\partial F_z}{\partial\rho}\right]+\alpha F_z+iaG_z=0 ,$$

$$\frac{1}{\rho}\frac{\partial}{\partial\rho}\left[\rho\frac{\partial G_z}{\partial\rho}\right]-\gamma G_z-ia\epsilon_\parallel F_z=0 , \tag{5}$$

where

$$\alpha\equiv-\epsilon_\parallel(x^2-\sigma^2\epsilon_\perp)/\epsilon_\perp ,$$

$$\gamma\equiv x^2-\sigma^2\epsilon_\perp(1-g^2/\epsilon_\perp^2) ,$$

$$a\equiv x\sigma g/\epsilon_\perp .$$

In Eqs. (5) all terms of $O((1/k)(\partial/\partial z)\ln H)$ (H being F_z, G_z, $\epsilon_\parallel$, $\epsilon_\perp$, g, or k) have been neglected. We seek the solutions to (5) using the ansatz

$$F_z(\rho)=f\frac{J_0(a_p\rho)}{J_0(a_p)}$$

and

$$G_z(\rho)=h\frac{J_0(a_p\rho)}{J_0(a_p)} ,$$

which immediately yields

$$\begin{aligned} F_z^p(\rho)&=f_1\frac{J_0(a_{p1}\rho)}{J_0(a_{p1})}+f_2\frac{J_0(a_{p2}\rho)}{J_0(a_{p2})} , \\ G_z^p(\rho)&=f_1\chi_1\frac{J_0(a_{p1}\rho)}{J_0(a_{p1})}+f_2\chi_2\frac{J_0(a_{p2}\rho)}{J_0(a_{p2})} , \end{aligned} \tag{6}$$

where

$$a_{p1,2}=(\tfrac{1}{2}\{\alpha-\gamma\pm[(\alpha+\gamma)^2+4a^2\epsilon_\parallel]^{1/2}\})^{1/2} \tag{7}$$

and

$$\begin{aligned} \chi_1&\equiv\frac{h}{f}\bigg|_{a_p=a_{p1}}=i\frac{\alpha-a_{p1}^2}{a}=iG_1 , \\ \chi_2&\equiv\frac{h}{f}\bigg|_{a_p=a_{p2}}=i\frac{\alpha-a_{p2}^2}{a}=iG_2 . \end{aligned} \tag{8}$$

Having derived the F_z and G_z components, from Maxwell's equations (2) one can obtain all other wave components, in particular

$$\begin{aligned} F_r^p(\rho)&=\frac{i}{x}\left[\frac{f_1}{a_{p1}}(a_{p1}^2-\epsilon_\parallel\sigma^2)\frac{J_1(a_{p1}\rho)}{J_0(a_{p1})}\right. \\ &\quad\left.+\frac{f_2}{a_{p2}}(a_{p2}^2-\epsilon_\parallel\sigma^2)\frac{J_1(a_{p2}\rho)}{J_0(a_{p2})}\right] , \\ G_r^p(\rho)&=x\left[G_1\frac{f_1}{a_{p1}}\frac{J_1(a_{p1}\rho)}{J_0(a_{p1})}+G_2\frac{f_2}{a_{p2}}\frac{J_1(a_{p2}\rho)}{J_0(a_{p2})}\right] , \\ F_\varphi^p(\rho)&=-\sigma\left[G_1\frac{f_1}{a_{p1}}\frac{J_1(a_{p1}\rho)}{J_0(a_{p1})}+G_2\frac{f_2}{a_{p2}}\frac{J_1(a_{p2}\rho)}{J_0(a_{p2})}\right] , \\ G_\varphi^p(\rho)&=-i\epsilon_\parallel\sigma\left[\frac{f_1}{a_{p1}}\frac{J_1(a_{p1}\rho)}{J_0(a_{p1})}+\frac{f_2}{a_{p2}}\frac{J_1(a_{p2}\rho)}{J_0(a_{p2})}\right] . \end{aligned} \tag{9}$$

In (6) and (9) J_0 and J_1 are the Bessel functions.

For vacuum, from Maxwell's equations one obtains the wave equations, whose solutions yield the axial wave-field components

$$F_z^v(\rho)=A\frac{K_0(a_v\rho)}{K_0(a_v)}$$

and

$$G_z^v(\rho)=iC\frac{K_0(a_v\rho)}{K_0(a_v)} , \tag{10}$$

where $a_v=(x^2-\sigma^2)^{1/2}$. The azimuthal wave components in vacuum have the simple form

$$F_\varphi^v(\rho)=\frac{\sigma}{a_v}C\frac{K_1(a_v\rho)}{K_0(a_v)}$$

and

$$G_\varphi^v(\rho)=i\frac{\sigma}{a_v}A\frac{K_1(a_v\rho)}{K_0(a_v)} , \tag{11}$$

while the radial ones, respectively, are

$$F_r^v(\rho)=i\frac{x}{a_v}A\frac{K_1(a_v\rho)}{K_0(a_v)}$$

and

$$G_r^v(\rho)=-\frac{x}{a_v}C\frac{K_1(a_v\rho)}{K_0(a_v)} . \tag{12}$$

Here K_0 and K_1 are the modified Bessel functions of the second kind, and A and C are constants. We notice that one assumes that the argument a_v is a real number, which means that the electromagnetic wave is a slow one—$v_{\rm ph}\equiv\omega/k<c$.

By imposing the boundary conditions (3) we find the following local dispersion relation of an electromagnetic wave traveling on a plasma column immersed in a constant magnetic field:

$$\frac{\left[\frac{1}{a_v}\frac{K_1(a_v)}{K_0(a_v)}+\frac{\epsilon_\parallel}{a_{p1}}\frac{J_1(a_{p1})}{J_0(a_{p1})}\right]\left[\frac{1}{a_v}\frac{K_1(a_v)}{K_0(a_v)}+\frac{1}{a_{p2}}\frac{J_1(a_{p2})}{J_0(a_{p2})}\right]}{\left[\frac{1}{a_v}\frac{K_1(a_v)}{K_0(a_v)}+\frac{\epsilon_\parallel}{a_{p2}}\frac{J_1(a_{p2})}{J_0(a_{p2})}\right]\left[\frac{1}{a_v}\frac{K_1(a_v)}{K_0(a_v)}+\frac{1}{a_{p1}}\frac{J_1(a_{p1})}{J_0(a_{p1})}\right]}=\frac{G_1}{G_2} . \tag{13}$$

Boundary conditions (3) allow us to obtain also the expressions for the coefficients f_1 and f_2, namely

$$f_1=\frac{\Delta(\omega,a_{p2})}{\epsilon_\parallel\Delta(a_{p1},a_{p2})}$$

and

$$f_2=-\frac{\Delta(\omega,a_{p1})}{\epsilon_\parallel\Delta(a_{p1},a_{p2})} , \tag{14}$$

where

$$\Delta(a_{p1},a_{p2})\equiv\frac{1}{a_{p2}}\frac{J_1(a_{p2})}{J_0(a_{p2})}-\frac{1}{a_{p1}}\frac{J_1(a_{p1})}{J_0(a_{p1})} ,$$

and

$$\Delta(\omega,a_p)\equiv\frac{1}{a_v}\frac{K_1(a_v)}{K_0(a_v)}+\frac{\epsilon_\parallel}{a_p}\frac{J_1(a_p)}{J_0(a_p)} .$$

We note that the equation $\Delta(\omega,a_p)=0$ would give us the dispersion relationship of pure TM surface of pseudosur-

face waves propagating along the column.

Dispersion relation (13) govern the propagation of a *generalized surface mode* in cylindrical geometry. Recently Ivanov, Alexov, and Malinov [36] presented the dispersion relation of symmetrical electromagnetic waves in a partially filled plasma waveguide (Eq. (4) in Ref. [36]). In the limit of absence of any metal tube their equation is equivalent to our (13) if, however, one corrects three misprints: namely, the comma on the first line of Eq. (4) is superfluous; on the second line a factor of ϵ_2 should be inserted in front of β_{3-i}; and the index i of k in the expression $P_0(k_i a)$ must be replaced with $3-i$. We note that it is straightforward to generalize (13) for the case of a plasma column of radius R surrounded by a metal tube or screen of radius R_1—in that case, by assuming the basic wave-field components in the vacuum in the form

$$F_z^v(\rho)=A\frac{K_0(a_v\rho)}{K_0(a_v)}+B\frac{I_0(a_v\rho)}{I_0(a_v)} ,$$

$$G_z^v(\rho)=iC\frac{K_0(a_v\rho)}{K_0(a_v)}+iD\frac{I_0(a_v\rho)}{I_0(a_v)} ,$$

and by imposing the additional boundary condition

$$F_z^v=F_\varphi^v=0 \quad \text{at } \rho=\eta ,$$

where $\eta\equiv R_1/R$, one arrives at

$$\frac{\left[\frac{1}{a_v}V(a_v)+\frac{\epsilon_\parallel}{a_{p1}}\frac{J_1(a_{p1})}{J_0(a_{p1})}\right]\left[\frac{1}{a_v}W(a_v)+\frac{1}{a_{p2}}\frac{J_1(a_{p2})}{J_0(a_{p2})}\right]}{\left[\frac{1}{a_v}V(a_v)+\frac{\epsilon_\parallel}{a_{p2}}\frac{J_1(a_{p2})}{J_0(a_{p2})}\right]\left[\frac{1}{a_v}W(a_v)+\frac{1}{a_{p1}}\frac{J_1(a_{p1})}{J_0(a_{p1})}\right]}=\frac{G_1}{G_2} , \tag{15}$$

where

$$V(a_v)=[K_1(a_v)+K_0(\eta a_v)I_1(a_v)/I_0(\eta a_v)]/[K_0(a_v)-K_0(\eta a_v)I_0(a_v)/I_0(\eta a_v)] ,$$

$$W(a_v)=[K_1(a_v)-K_1(\eta a_v)I_1(a_v)/I_1(\eta a_v)]/[K_0(a_v)+K_1(\eta a_v)I_0(a_v)/I_1(\eta a_v)] ,$$

and I_0 and I_1 are the modified Bessel functions of the first kind. Obviously, Eq. (15) is more compact and readable than Eq. (4) in Ref. [36]. Now, the equation

$$\frac{1}{a_v}V(a_v)+\frac{\epsilon_\parallel}{a_p}\frac{J_1(a_p)}{J_0(a_p)}=0$$

would present the dispersion relation of a pure surface or pseudosurface electromagnetic mode in a partially filled plasma waveguide—in the limit $\eta\to\infty$, $V(a_v)$ and $W(a_v)$ tend to $K_1(a_v)/K_0(a_v)$, i.e., (15) passes into (13). Equation (13) naturally includes the simpler cases as follows.

A. Absence of an external magnetic field ($\mathbf{B}_0=0$)

In this case $g=0$, $\epsilon_\perp=\epsilon_\parallel=\epsilon$, $a_{p1}\equiv a_{p2}=i(x^2-\epsilon\sigma^2)^{1/2}$, $G_1+G_2\to 0$ as $g\to 0$, and one obtains the dispersion relation of a pure surface mode [27]

$$\frac{1}{a_v}\frac{K_1(a_v)}{K_0(a_v)}+\frac{\epsilon}{a_p}\frac{I_1(a_p)}{I_0(a_p)}=0 \tag{16}$$

with $f_1=f_2=0.5$. Now we have only three wave components:

$$\mathcal{E}_z^p(\rho)=\frac{I_0(a_p\rho)}{I_0(a_p)}\mathcal{E}, \quad \mathcal{E}_r^p(\rho)=-i\frac{x}{a_p}\frac{I_1(a_p\rho)}{I_0(a_p)}\mathcal{E} ,$$

and

$$\mathcal{B}_\varphi^p(\rho)=-\frac{i\epsilon\sigma}{a_p}\frac{I_1(a_p\rho)}{I_0(a_p)}\mathcal{E} .$$

B. Electrostatic limit ($\mathbf{B}_0\neq 0$)

In that case $\sigma=0$, $a=0$, $a_{p1}\equiv\xi=(-\epsilon_\parallel x^2/\epsilon_\perp)^{1/2}$, $a_{p2}=ix$, $a_v=x$, $G_1\to 0$, $G_2\to-\infty$, and the wave dispersion relation becomes [32]

$$\frac{1}{x}\frac{K_1(x)}{K_0(x)}+\frac{\epsilon_\parallel}{\xi}\frac{J_1(\xi)}{J_0(\xi)}=0 . \tag{17}$$

For $\Omega\equiv\omega_c/\omega>1$ the wave is a pseudosurface mode, while for $\Omega<1$ it is a pure surface one. In both situations $f_1=1$ and $f_2=0$, and the only wave components are

$$\mathcal{E}_z^p(\rho)=\frac{J_0(\xi\rho)}{J_0(\xi)}\mathcal{E}$$

and

$$\mathcal{E}_r^p(\rho)=i\frac{\xi}{x}\frac{J_1(\xi\rho)}{J_0(\xi)}\mathcal{E} .$$

C. Infinite external magnetic field ($\mathbf{B}_0\to\infty$)

In this limit, $\epsilon_\perp\to 1$, $g\to-0$, $a_{p1}=\sqrt{-\epsilon_\parallel}a_v$, $a_{p2}=ia_v$, $G_1=0$, $G_2\to-\infty$, and Eq. (13) reduces to

$$\sqrt{-\epsilon_\parallel}\frac{J_1(\sqrt{-\epsilon_\parallel}a_v)}{J_0(\sqrt{-\epsilon_\parallel}a_v)}-\frac{K_1(a_v)}{K_0(a_v)}=0 , \tag{18}$$

which is the dispersion relation of a pure TM pseudosurface mode. Now $f_1=1$, $f_2=0$, with

$$\mathcal{E}_z^p(\rho)=\frac{J_0(\sqrt{-\epsilon_\parallel}a_v\rho)}{J_0(\sqrt{-\epsilon_\parallel}a_v)}\mathcal{E}\ ,$$

$$\mathcal{E}_r^p(\rho)=i\sqrt{-\epsilon_\parallel}\frac{x}{a_v}\frac{J_1(\sqrt{-\epsilon_\parallel}a_v\rho)}{J_0(\sqrt{-\epsilon_\parallel}a_v)}\mathcal{E}\ ,$$

and

$$\mathcal{B}_\varphi^p(\rho)=i\sqrt{-\epsilon_\parallel}\frac{\sigma}{a_v}\frac{J_1(\sqrt{-\epsilon_\parallel}a_v\rho)}{J_0(\sqrt{-\epsilon_\parallel}a_v)}\mathcal{E}\ .$$

The high-frequency generalized surface-wave-energy-balance equation is derived from Poynting's theorem for both media making use of the boundary conditions (3). It takes the simple form

$$\frac{d}{dz}S=-Q\ , \tag{19}$$

where S is the wave power and Q is the absorbed power per unit length. The former can be represented as a sum of the axial components of Poynting's vector averaged over the wave period $2\pi/\omega$ and integrated over the plane normal to the plasma column, from the axis to infinity, at a given axial position z. It is

$$\begin{aligned}
S=&\frac{c}{8\pi}\left[2\pi\,\mathrm{Re}\int_0^R dr\,r(\mathcal{E}_r^{p*}\mathcal{B}_\varphi^p-\mathcal{E}_\varphi^{p*}\mathcal{B}_r^p)+2\pi\,\mathrm{Re}\int_R^\infty dr\,r(\mathcal{E}_r^{v*}\mathcal{B}_\varphi^v-\mathcal{E}_\varphi^{v*}\mathcal{B}_r^v)\right]\\
=&\frac{\omega}{4}R^3\mathcal{E}^2\left[\frac{f_1^*f_1}{(a_{p1}^*)^2-a_{p1}^2}\left[\frac{N-1}{x}[(a_{p1}^*)^2+\sigma^2(N-1)]+xG_1^*G_1\right]\left[\frac{1}{a_{p1}^*}\frac{J_1(a_{p1}^*)}{J_0(a_{p1}^*)}-\frac{1}{a_{p1}}\frac{J_1(a_{p1})}{J_0(a_{p1})}\right]\right.\\
&+\frac{f_2^*f_1}{(a_{p2}^*)^2-a_{p1}^2}\left[\frac{N-1}{x}[(a_{p2}^*)^2+\sigma^2(N-1)]+xG_2^*G_1\right]\left[\frac{1}{a_{p2}^*}\frac{J_1(a_{p2}^*)}{J_0(a_{p2}^*)}-\frac{1}{a_{p1}}\frac{J_1(a_{p1})}{J_0(a_{p1})}\right]\\
&+\frac{f_1^*f_2}{(a_{p1}^*)^2-a_{p2}^2}\left[\frac{N-1}{x}[(a_{p1}^*)^2+\sigma^2(N-1)]+xG_1^*G_2\right]\left[\frac{1}{a_{p1}^*}\frac{J_1(a_{p1}^*)}{J_0(a_{p1}^*)}-\frac{1}{a_{p2}}\frac{J_1(a_{p2})}{J_0(a_{p2})}\right]\\
&+\frac{f_2^*f_2}{(a_{p2}^*)^2-a_{p2}^2}\left[\frac{N-1}{x}[(a_{p2}^*)^2+\sigma^2(n-1)]+xG_2^*G_2\right]\left[\frac{1}{a_{p2}^*}\frac{J_1(a_{p2}^*)}{J_0(a_{p2}^*)}-\frac{1}{a_{p2}}\frac{J_1(a_{p2})}{J_0(a_{p2})}\right]\\
&\left.+\frac{1}{2}(1+C^*C)\frac{x}{a_v^2}\left[1-\frac{K_1^2(a_v)}{K_0^2(a_v)}+\frac{2}{a_v}\frac{K_1(a_v)}{K_0(a_v)}\right]\right]\ ,
\end{aligned}\tag{20}$$

where $C=f_1G_1+f_2G_2$. As usual, the asterisk denotes a complex conjugate. Note that at any given position z along the discharge tube $S(z)$ is the wave power necessary to sustain the rest of the plasma column, as we assume that at the end of the column $S(z_{\mathrm{end}})=0$. The absorbed power per unit length is

$$\begin{aligned}
Q=&2\pi\int_0^R dr\,r\langle\mathbf{j}\cdot\mathbf{E}\rangle=i\frac{\omega}{8}(\epsilon_{ij}^*-\epsilon_{ji})\int_0^R dr\,r\,\mathcal{E}_i\mathcal{E}_j^*\\
=&\frac{\omega}{4}\int_0^R dr\,r[\mathrm{Im}(\tilde{\epsilon}_\perp)(|\mathcal{E}_r^p|^2+|\mathcal{E}_\varphi^p|^2)+\mathrm{Im}(\tilde{\epsilon}_\parallel)|\mathcal{E}_z^p|^2+i\,\mathrm{Im}(\tilde{g})(\mathcal{E}_r^p\mathcal{E}_\varphi^{p*}-\mathcal{E}_\varphi^p\mathcal{E}_r^{p*})]\\
=&\frac{1}{4}\nu NR^2\mathcal{E}^2\left\{\frac{f_1^*f_1}{(a_{p1}^*)^2-a_{p1}^2}\left[\frac{1}{a_{p1}^*}\frac{J_1(a_{p1}^*)}{J_0(a_{p1}^*)}-\frac{1}{a_{p1}}\frac{J_1(a_{p1})}{J_0(a_{p1})}\right]\right.\\
&\times\left[\frac{1+\Omega^2}{(1-\Omega^2)^2}\left[\frac{1}{x^2}[(a_{p1}^*)^2+\sigma^2(N-1)][a_{p1}^2+\sigma^2(N-1)]+\sigma^2G_1^*G_1\right]\right.\\
&\left.\left.-2\frac{\sigma\Omega}{(1-\Omega^2)^2}\frac{1}{x}\{G_1^*[a_{p1}^2+\sigma^2(N-1)]+G_1[(a_{p1}^*)^2+\sigma^2(N-1)]\}\right]\\
&+\frac{f_2^*f_1}{(a_{p2}^*)^2-a_{p1}^2}\left[\frac{1}{a_{p2}^*}\frac{J_1(a_{p2}^*)}{J_0(a_{p2}^*)}-\frac{1}{a_{p1}}\frac{J_1(a_{p1})}{J_0(a_{p1})}\right]\\
&\times\left[\frac{1+\Omega^2}{(1-\Omega^2)^2}\left[\frac{1}{x^2}[(a_{p2}^*)^2+\sigma^2(N-1)][a_{p1}^2+\sigma^2(N-1)]+\sigma^2G_2^*G_1\right]\right.\\
&\left.-2\frac{\sigma\Omega}{(1-\Omega^2)^2}\frac{1}{x}\{G_2^*[a_{p1}^2+\sigma^2(N-1)]+G_1[(a_{p2}^*)^2+\sigma^2(n-1)]\}\right]\\
&+\frac{f_1^*f_2}{(a_{p1}^*)^2-a_{p2}^2}\left[\frac{1}{a_{p1}^*}\frac{J_1(a_{p1}^*)}{J_0(a_{p1}^*)}-\frac{1}{a_{p2}}\frac{J_1(a_{p2})}{J_0(a_{p2})}\right]
\end{aligned}$$

$$\times\left[\frac{1+\Omega^2}{(1-\Omega^2)^2}\left[\frac{1}{x^2}[(a_{p1}^*)^2+\sigma^2(N-1)][a_{p2}^2+\sigma^2(N-1)]+\sigma^2 G_1^* G_2\right]\right.$$
$$\left.-2\frac{\sigma\Omega}{(1-\Omega^2)^2}\frac{1}{x}\{G_1^*[a_{p2}^2+\sigma^2(N-1)]+G_2[(a_{p1}^*)^2+\sigma^2(N-1)]\}\right]$$
$$+\frac{f_2^* f_2}{(a_{p2}^*)^2-a_{p2}^2}\left[\frac{1}{a_{p2}^*}\frac{J_1(a_{p2}^*)}{J_0(a_{p2}^*)}-\frac{1}{a_{p2}}\frac{J_1(a_{p2})}{J_0(a_{p2})}\right]$$
$$\times\left[\frac{1+\Omega^2}{(1-\Omega^2)^2}\left[\frac{1}{x^2}[(a_{p2}^*)^2+\sigma^2(N-1)][a_{p2}^2+\sigma^2(n-1)]+\sigma^2 G_2^* G_2\right]\right.$$
$$\left.-2\frac{\sigma\Omega}{(1-\Omega^2)^2}\frac{1}{x}\{G_2^*[a_{p2}^2+\sigma^2(N-1)]+G_2[(a_{p2}^*)^2+\sigma^2(n-1)]\}\right]$$
$$+\frac{f_1^* f_1}{(a_{p1}^*)^2-a_{p1}^2}\left[a_{p1}^*\frac{J_1(a_{p1}^*)}{J_0(a_{p1}^*)}-a_{p1}\frac{J_1(a_{p1})}{J_0(a_{p1})}\right]+\frac{f_2^* f_1}{(a_{p2}^*)^2-a_{p1}^2}\left[a_{p2}^*\frac{J_1(a_{p2}^*)}{J_0(a_{p2}^*)}-a_{p1}\frac{J_1(a_{p1})}{J_0(a_{p1})}\right]$$
$$+\frac{f_1^* f_2}{(a_{p1}^*)^2-a_{p2}^2}\left[a_{p1}^*\frac{J_1(a_{p1}^*)}{J_0(a_{p1}^*)}-a_{p2}\frac{J_1(a_{p2})}{J_0(a_{p2})}\right]+\frac{f_2^* f_2}{(a_{p2}^*)^2-a_{p2}^2}\left[a_{p2}^*\frac{J_1(a_{p2}^*)}{J_0(a_{p2}^*)}-a_{p2}\frac{J_1(a_{p2})}{J_0(a_{p2})}\right]\Bigg\}, \tag{21}$$

where ϵ_{ij}^* and ϵ_{ji} are the elements of the tensor $\overleftrightarrow{\epsilon}^p$. In formula (21), the angular brackets denote an averaging over the wave period.

In order to find out the axial distributions of the electron number density n, the wave number k, the wave-field components, and the wave power S, we need one more equation. Such an equation can be derived from the following considerations: the wave power absorbed per unit length (Q) serves, under steady-state conditions, to maintain electron thermal energy, which is expended in excitation, ionization, heating of the neutral gas, maintaining a negative wall potential, etc. If the plasma is produced primarily by single-step ionization (the rate of ionization is then proportional to n) and if the main electron loss process is the diffusion of charged particles to the wall (diffusion regime), in such a case $Q \propto n$. When two-step ionization and dissociative and/or bulk recombination processes are dominant (the rates are proportional to n^s, where $1<s\leq 3$), we have approximately $Q \propto n^s$, and the gas-discharge regime is called a recombination one. All these relations between Q and n can be incorporated into one equation using the dimensionless variable N and the number $\beta=s-1$ [32]:

$$Q=Q_\beta N^{1+\beta}, \tag{22}$$

where Q_β is a constant of proportionality that does not depend on the axial position. Q_β may be determined from an exact electron thermal energy-balance equation. The different values of β correspond to different gas-discharge conditions, namely $\beta=0$ (free fall or diffusion regime) and $0<\beta\leq 2$ (bulk recombination regime). Relations (13), (19), and (22) constitute our basic set of equations.

Equation (19), with the help of expressions (20) and (22), can be rewritten in a more convenient form by using the dimensionless axial coordinate $\zeta=\nu z/\omega R$:

$$\frac{dS_*}{d\zeta}=-N^{1+\beta}, \tag{23}$$

where the dimensionless wave power $S_*=S/(\omega R Q_\beta/\nu)$ is

$$S_*=2E_*^2 L, \tag{24}$$

L being the long expression in the large square brackets of (20). Here, the normalized axial wave electric-field component at the plasma-vacuum interface $E_*(x,N)=\mathcal{E}/(8Q_\beta/\nu R^2)^{1/2}$ is determined from (21) and (22), and its square is

$$E_*^2=N^\beta/2H, \tag{25}$$

where H is the expression in the large curly brackets of (21). Let us note that now the axial profiles of the dimensionless electron number density N, the wave power S_*, the wave number x, and all the wave-field components are specified by the two equations (13) and (23).

The axial structure of the column plasma density as well as the electromagnetic wave characteristics in the limit of an infinite magnetic field ($B_0\rightarrow\infty$) should be determined by much simpler equations. In that limit, first, the wave is a pure TM mode whose propagation is governed by the dispersion relation (18). Secondly, the expressions for S and Q, which follow from (20) and (21) as $\Omega\rightarrow\infty$, respectively, are

$$S_\infty=\frac{\omega}{4}R^3E^2\left\{\frac{x}{2a_v^2}\left[(N-1)\left[1+\frac{J_1^2(\xi)}{J_0^2(\xi)}-\frac{2}{\xi}\frac{J_1(\xi)}{J_0(\xi)}\right]\right.\right.$$
$$\left.\left.+1-\frac{K_1^2(a_v)}{K_0^2(a_v)}+\frac{2}{a_v}\frac{K_1(a_v)}{K_0(a_v)}\right]\right\} \tag{26}$$

and

$$Q_\infty = \frac{1}{4}\nu N R^2 \mathcal{E}^2 \left[\frac{1}{2}\left[1+\frac{J_1^2(\xi)}{J_0^2(\xi)}\right]\right], \quad (27)$$

where $\xi=\sqrt{-\epsilon_\parallel}a_v$. The corresponding dimensionless wave power $S_{*\infty}$ (and the squared normalized axial wave-electric-field component at the plasma-vacuum interface $E^2_{*\infty}$), which should enter Eq. (23), now become

$$S_{*\infty} = E^2_{*\infty} x \left[(N-1)\left[1+\frac{J_1^2(\xi)}{J_0^2(\xi)}-\frac{2}{\xi}\frac{J_1(\xi)}{J_0(\xi)}\right] +1-\frac{K_1^2(a_v)}{K_0^2(a_v)}+\frac{2}{a_v}\frac{K_1(a_v)}{K_0(a_v)}\right]\Big/ a_v^2 , \quad (28)$$

where

$$E^2_{*\infty} = N^\beta/[1+J_1^2(\xi)/J_0^2(\xi)] . \quad (29)$$

Expression (28), with the help of dispersion relation (18), may be reduced to the form

$$S_{*\infty} = E^2_{*\infty} x N / a_v^2 , \quad (28')$$

which, naturally, generalizes the simplest form of $S_{*\infty}$ in the electrostatic limit $\sigma\to 0$ (c.f. expression (23) in Ref. [32]).

IV. NUMERICAL SOLVING OF THE BASIC SET OF EQUATIONS AND RESULTS

The axial structure of the plasma column density, electromagnetic wave-field components, and dispersion characteristics are specified by the two basic equations (13) and (23). The manner of their resolution is the following: from the local-dispersion relation (13), for a fixed value of z (or ζ), one can obtain the dependence of the dimensionless electron number density N on the normalized wave number x, $N=N(x)$. Further on, that relation is introduced into the right-hand side of the differential equation (23) and the latter is solved numerically. We note that the equations (13) and (23) contain Bessel functions with arguments $a_{p1,2}$ and a_v. If $a_v=(x^2-\sigma^2)^{1/2}$ is always real, the values of $a_{p1,2}$ given by expression (7) might be real, imaginary, or complex conjugate, depending on the external magnetic field B_0 (respectively Ω), the wave frequency ω and column radius R (or σ) and the local magnitude of the electron number density n (or N). As $\Omega<1$ (a "weak magnetic field" [32]) the arguments $a_{p1,2}$ are complex conjugate or imaginary depending on the value of z. With high enough wave power (respectively long columns), $a_{p1,2}$ near the exciter should be complex conjugate, becoming at some z to the end of the column imaginary. For short plasma columns it is possible for the arguments $a_{p1,2}$ to be only imaginary in the whole region from the exciter to the column end. In the opposite case, $\Omega>1$ (a "strong magnetic field" [32]) the situation is more complicated—along the column length $a_{p1,2}$ might be complex conjugate, both real (or imaginary), and one real, the other imaginary depending on the particular values of Ω, σ, and z. This means that, propagating along the column, the wave changes its character and may be a generalized surface mode, pure surface mode, or a pseudosurface one [32,34]. For an infinite magnetic field ($\Omega\to\infty$) the electromagnetic wave is a TM pseudosurface mode everywhere.

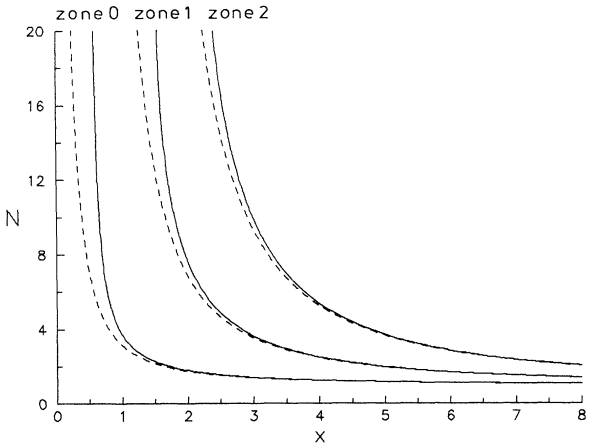

FIG. 2. Phase diagrams in the zero, first, and second zones at $\Omega=5$ (strong magnetic field) for $\sigma=0$ (dashed curves) and $\sigma=0.5$ (solid curves).

Due to the specific character of the arguments $a_{p1,2}$ expressions (20) and (21) for S and Q cannot be used directly for numerical calculations, since some of the denominators, for given $a_{p1,2}$, become equal to zero. In those cases the corresponding expressions, obtained from integrals of the kind $\int dw\, w\, J_n(y_1 w)J_n(y_2 w)$, must be replaced with others calculated from $\int dw\, w\, J_n^2(yw)$.

As in the case of electrostatic waves [32], for $\Omega>1$, dispersion relation (13) possesses multivalued solutions $N(x)$. In Fig. 2 we present the phase curves [$N=N(x)$ at fixed ω] in the zero, first, and second zones for $\Omega=5$ and for two values of σ: $\sigma=0$ (electrostatic limit, dashed curves) and $\sigma=0.5$ (solid curves). The influence of the parameter σ is strongest in the zero zone and it decreases with the increase of the zone number. A similar situation is valid for an infinite magnetic field ($\Omega\to\infty$), too.

The axial profiles of the normalized electron number density N for the zero, first, and second zones in the diffusion gas-discharge regime ($\beta=0$) for the same values of Ω and σ are shown in Fig. 3. As one sees from this figure, the influence of the parameter σ on the axial profiles of N is visible only in the zero zone—in the other zones there is not practically any difference. The same is valid also for the wave power S_*. However, σ changes the course of the wave number $x(\zeta)$ as well as the course of the wave-electric-field components in all zones. The situation is similar for the case of a recombination gas-discharge regime, as well as in the limit of an infinite external magnetic field ($\Omega\to\infty$).

From an experimental point of view, only the zero zone is interesting. Up to now there have been no results concerning the sustaining of a plasma column due to waves corresponding to the other zones. The axial profiles of the dimensionless electron number density, wave number, wave power, and wave-field components in the zero zone have been calculated for two different gas-

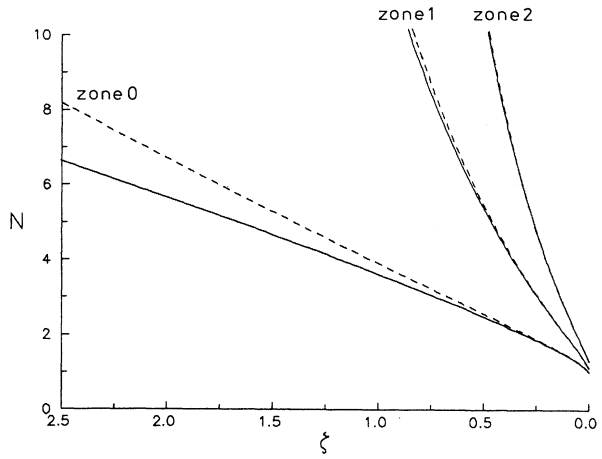

FIG. 3. Calculated axial profiles of the normalized electron number density $N(\zeta)$ for $\sigma=0$ (dashed curves) and $\sigma=0.5$ (solid curves) in the free fall and/or diffusion gas-discharge regime ($\beta=0$) for a strong magnetic field ($\Omega=5$) within the zero, first, and second zones.

discharge conditions [diffusion regime ($\beta=0$) and recombination one ($\beta=1$), respectively]. They depend on the two parameters σ and Ω. The dependence of all the profiles on Ω at a fixed value of σ ($=0.5$) for a diffusion regime can be seen in Figs. 4–8. These figures include curves, calculated both for weak magnetic fields ($\Omega<1$) and strong fields ($\Omega>1$), as well as for the case of an isotropic plasma ($\Omega=0$) and an infinite external magnetic field ($\Omega\rightarrow\infty$). The curves, associated with the latter two cases, are plotted as dashed lines. One sees that the influence of a weak magnetic field on the plasma density axial profile and on the structure of the electromagnetic wave is negligibly small. The strong magnetic field ($\Omega\geq 2.5$) changes both the wave characteristics and the axial plasma density gradient. The dependence of the

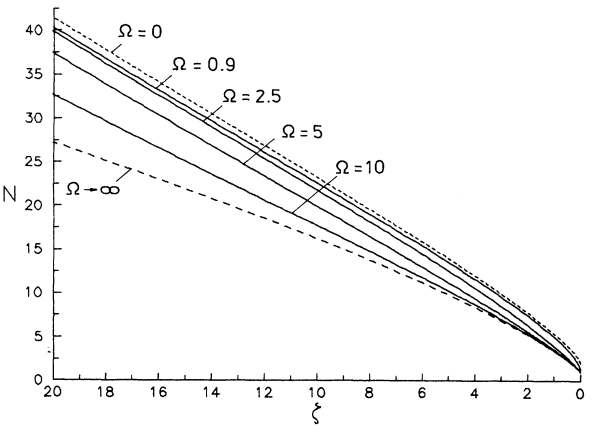

FIG. 4. Calculated axial profiles of the normalized electron number density $N(\zeta)$ for $\sigma=0.5$ in the free fall and/or diffusion gas-discharge regime ($\beta=0$) for different magnetic fields ($\Omega=0.9$, 2.5, 5, and 10). The dashed curves correspond to an isotropic plasma column ($\Omega=0$) and to an infinite external magnetic field ($\Omega\rightarrow\infty$), respectively.

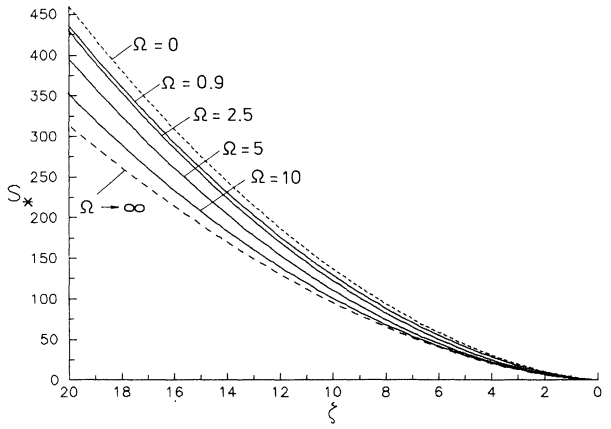

FIG. 5. Calculated axial profiles of the normalized wave power $S_*(\zeta)$ for the same conditions as in Fig. 4.

plasma density profile $N(\zeta)$ (Fig. 4), wave power $S_*(\zeta)$ (Fig. 5), and the wave-field components $E_z(\zeta)$ (Fig. 6) and $B_\varphi(\zeta)$ (Fig. 8) on the magnetic field Ω is monotonous and all these curves lie between the profiles corresponding to $\Omega=0$ and $\Omega\rightarrow\infty$. It follows from Fig. 4 that with the increase of the magnetic field, the dimensionless axial plasma density gradient decreases, and at a fixed value of N near the exciter the column length increases. The same conclusion is drawn from Fig. 5, too—at a fixed wave power near the wave exciter, the stronger the magnetic field, the longer the column length. We note that all the wave-field components are evaluated at the plasma-vacuum interface and they have been calculated as products of $F_{r,\varphi,z}$ or $G_{r,\varphi,z}$ with $E_*=\mathcal{E}/(8Q_\beta/\nu R^2)^{1/2}$.

The behavior of the wave-field components $E_r(\zeta)$, $E_\varphi(\zeta)$, $B_z(\zeta)$, and $B_r(\zeta)$ turns out to be quite irregular. For example, the E_r component (Fig. 7) decreases with the increase of Ω in the range 0–1.1; after that, the same component starts to increase. Moreover, at $\Omega=1.1$, the radial wave-electric-field component is generally very small; it even becomes almost zero at some distance from the end of the column [Fig. 7(b)]. It is interesting to note

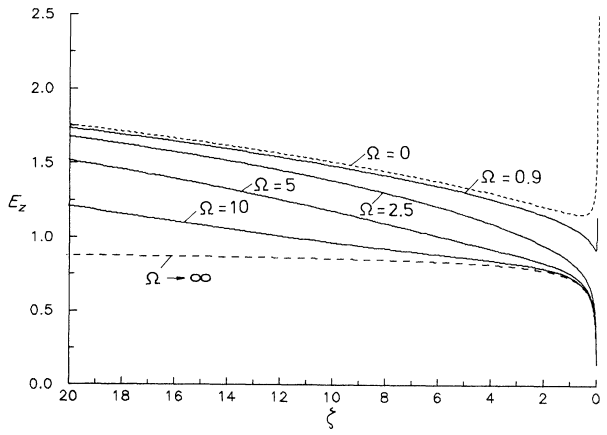

FIG. 6. Calculated axial profiles of the normalized $E_z(\zeta)$ wave-field component for the same conditions as in Fig. 4.

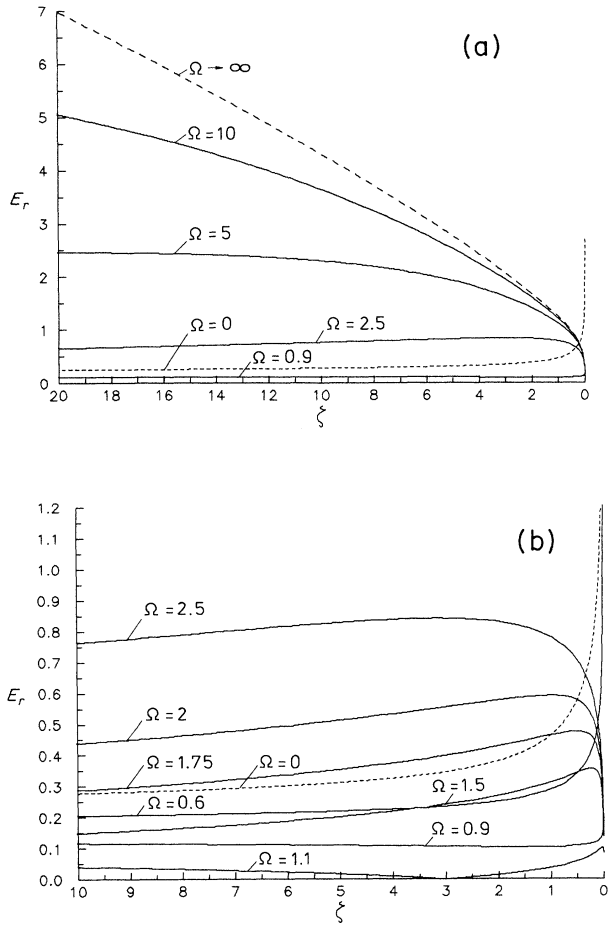

FIG. 7. Calculated axial profiles of the normalized $|E_r(\zeta)|$ wave-field component for (a) the same conditions as in Fig. 4 and (b) magnetic fields $\Omega=0$ (dashed), 0.6, 0.9, 1.1, 1.5, 1.75, 2, and 2.5 at $\sigma=0.5$ and $\beta=0$.

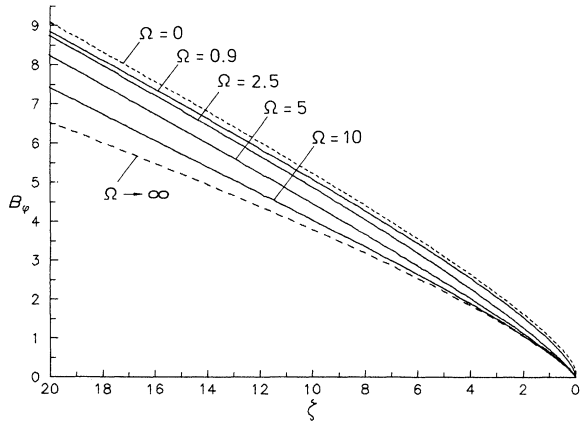

FIG. 8. Calculated axial profiles of the normalized $|B_\varphi(\zeta)|$ wave-field component for the same conditions as in Fig. 4.

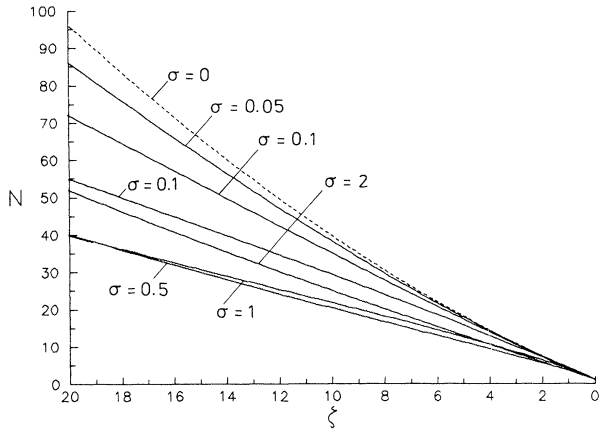

FIG. 9. Calculated axial profiles of the normalized electron number density $N(\zeta)$ at $\Omega=2.5$ (strong magnetic field) in the free fall and/or diffusion gas-discharge regime ($\beta=0$) for different values of the parameter σ (=0.05, 0.1, 0.2, 0.5, 1, and 2). The dashed curve corresponds to the electrostatic limit ($\sigma=0$).

that, in contrast to an isotropic plasma, for a strong magnetic field the E_r wave component plays an important role, since with the increase of Ω the E_z wave component decreases while E_r increases. In particular, for $\Omega \geq 5$, E_r becomes larger than E_z (c.f. Figs. 6 and 7). We emphasize that this model is not applicable to the case of electron cyclotron resonance ($\Omega=1$). However, it still works for values of Ω near 1—the curves for $\Omega=0.9$ and 1.1 lie very close. The end of the column occurs at $S_*=0$, which corresponds to [32]

$$N_{\text{resonance}} = \begin{cases} 2-\Omega^2 & \text{for } \Omega < 1 \\ 1 & \text{for } \Omega > 1 \end{cases}.$$

At fixed Ω (say, =2.5) all the axial profiles should depend on the value of σ. These profiles, except for those corresponding to $N(\zeta)$ and $S_*(\zeta)$, move upwards with the increase of σ. The dependence of $N(\zeta)$ (Fig. 9) and $S_*(\zeta)$ on σ is more complicated—for small values of σ ($\sigma<1$) with the increase of σ, the axial gradients of $N(\zeta)$ and $S_*(\zeta)$ decrease and next (for $\sigma>1$) increase. This behavior of $N(\zeta)$ and $S_*(\zeta)$ is similar to that for an isotropic surface-wave sustained plasma column [28]. It is worth pointing out that the $N(\zeta)$ profiles are generally *nonlinear* and one can define only some average density gradient for a given region of N. In Table I one can see the average slope of $N(\zeta)$ curves for $\sigma=0.5$, $\beta=0$ (diffusion regime) in the ranges $1<N\leq 10$ and $10\leq N\leq 30$ at different values of Ω. We would like to emphasize that while the E_z wave component in the electrostatic limit ($\sigma=0$) is practically constant ($\cong 1$) along the column length, in reality ($\sigma>0$) the situation is different—E_z decreases along z and for larger σ's it possesses higher values (Fig. 10). In that reason the dependence of the E_z electromagnetic wave component on the magnetic field (see Fig. 6) is not similar to that of an electrostatic wave [cf. Figs. 2(b) and 6(b) in Ref. 32].

TABLE I. Average values of the dimensionless plasma density slope $|dN/d\zeta|$ within the ranges $1 \le N \le 10$ and $10 \le N \le 30$ for free fall or diffusion ($\beta=0$) and recombination ($\beta=1$) gas-discharge regimes at $\sigma=0.5$ in strong magnetic fields ($\Omega>1$). For comparison, the first column gives the corresponding slopes of an isotropic plasma column ($\Omega=0$) with $\sigma=0.5$.

Ω	0		2.5		5		10		∞	
N	1–10	10–30	1–10	10–30	1–10	10–30	1–10	10–30	1–10	10–30
					$\beta=0$					
$\left\|\frac{dN}{d\zeta}\right\|$	2.62	1.86	2.41	1.84	2.07	1.74	1.86	1.49	1.76	1.15
					$\beta=1$					
$\left\|\frac{dN}{d\zeta}\right\|$	1.94	1.28	1.71	1.44	1.47	1.18	1.33	1.01	1.26	0.85

The analogous axial profiles for the same values of Ω and σ have been obtained for recombination gas-discharge conditions ($\beta=1$). The profiles depend in a similar way on σ and Ω, but there are some specific differences. The magnitude of N and its axial gradient for $\beta=1$ are lower in comparison with those for a column sustained at diffusion gas-discharge conditions (see Table I). The same regularity is valid also for an isotropic plasma column [28]. The wave power S_* is generally larger (at least of one order) than that at a diffusion regime and it decreases with a greater local axial gradient. Accordingly, all the components of the electromagnetic wave at recombination gas-discharge conditions are of one order larger than those of the diffusion regime. We note, however, that the ζ dependencies of the wave-field components for the two regimes are different. In particular, the B_φ wave component at the diffusion regime is a concave curve, while at recombination gas-discharge conditions it becomes a convex curve.

Due to the plasma anisotropy, the electromagnetic wave is neither a TM nor a TE mode—it possesses all the six components. Moreover, the radial profiles of the wave components do not correspond to pure surface or pure pseudosurface modes along the whole column length. Depending on the arguments of Bessel functions $a_{p1,2}$, one of the modes can dominate. If both arguments are imaginary, the wave is a surface one; if they are real, it is a pseudosurface wave. In the case when one of the arguments is real and the other is imaginary, the wave is a mixture of these two modes and possesses the character of the dominating mode. Finally, when the arguments are complex conjugate, the wave might be called a *generalized surface wave, since both modes participate equally in it.* For a given plasma column one may observe only a few of these possibilities depending on the values of Ω and σ and the gas-discharge conditions (respectively β).

In the case of a weak magnetic field ($\Omega<1$) for large σ's, the wave is practically a generalized surface mode, becoming a surface wave at the end of the column. As σ decreases that part of the column where the wave is a surface mode increases, and for $\sigma=0$ the wave is a pure surface mode everywhere [32]. At $\sigma=0.05$ and $\Omega=0.6$

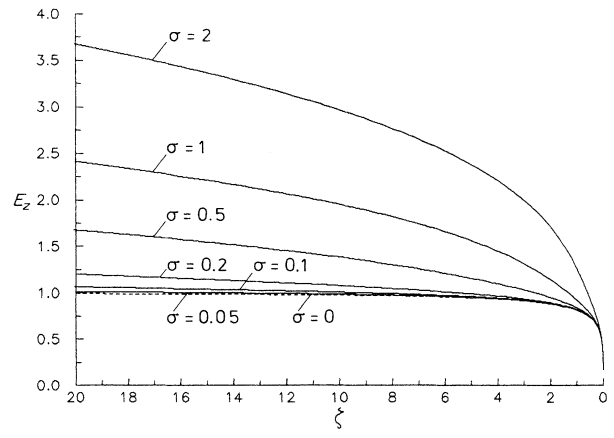

FIG. 10. Calculated axial profiles of the normalized $E_z(\zeta)$ wave-field component at $\Omega=2.5$ for the same conditions as in Fig. 9.

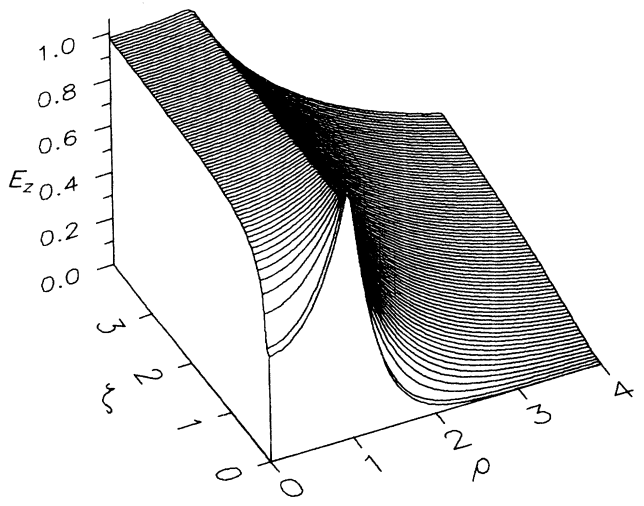

FIG. 11. Structure of the normalized $E_z(\rho,\zeta)$ wave-field component at $\sigma=0.05$ and $\Omega=0.6$ (weak magnetic field) in free fall or diffusion gas-discharge conditions ($\beta=0$).

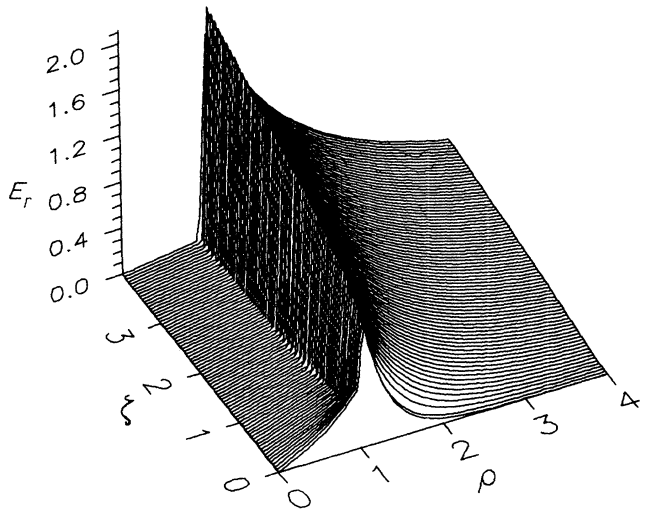

FIG. 12. Structure of the normalized $|E_r(\rho,\zeta)|$ wave-field component at $\sigma=0.05$ and $\Omega=0.6$ (weak magnetic field) in free fall or diffusion gas-discharge conditions ($\beta=0$).

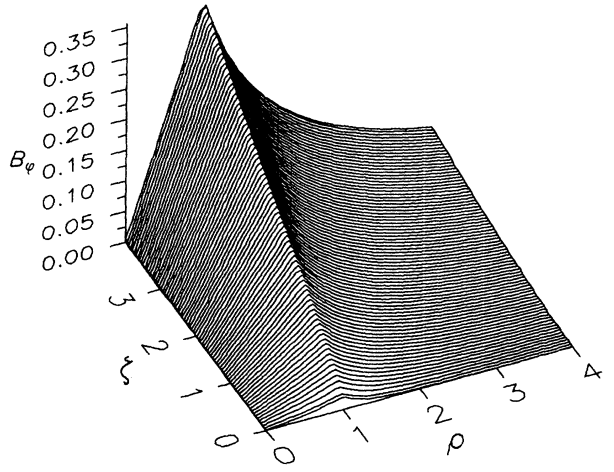

FIG. 14. Structure of the normalized $|B_\varphi(\rho,\zeta)|$ wave-field component at $\sigma=0.05$ and $\Omega=0.6$ (weak magnetic field) in free fall or diffusion gas-discharge conditions ($\beta=0$).

one can see the structure of both type of waves in Figs. 11–16, where we show three-dimensional plots of the E_z, E_r, B_z, and B_φ wave components as well as the total electric and magnetic wave fields—the view is from the end of the column to the wave exciter. We note that the B_z component, which is very small at the plasma-vacuum interface, becomes much larger into the column.

For a strong magnetic field ($\Omega>1$) at large σ's the wave normally is a generalized surface mode, which, near the end of the column, becomes a pseudosurface one. At small σ's and short columns, the wave is dominantly a pseudosurface mode—for $\sigma=0$ the wave is a pseudosurface mode everywhere [32]. The structures of the E_z and E_r wave components (for $\sigma=0.2$ and $\Omega=2.5$) are shown in Figs. 17 and 18. The structure of the B_z and B_φ components is similar to that for the case of a weak magnetic field, but now their magnitude is of one order larger. The total electric and magnetic fields are shown in Figs. 19 and 20.

We note that the E_φ and B_r wave components in both cases are generally small quantities, and they have their largest magnitudes at the plasma-vacuum interface, being equal to zero at the column axis.

V. COMPARISON WITH THEORETICAL AND EXPERIMENTAL WORKS

The axial and radial profiles obtained here are in dimensionless quantities, while all known theoretical and

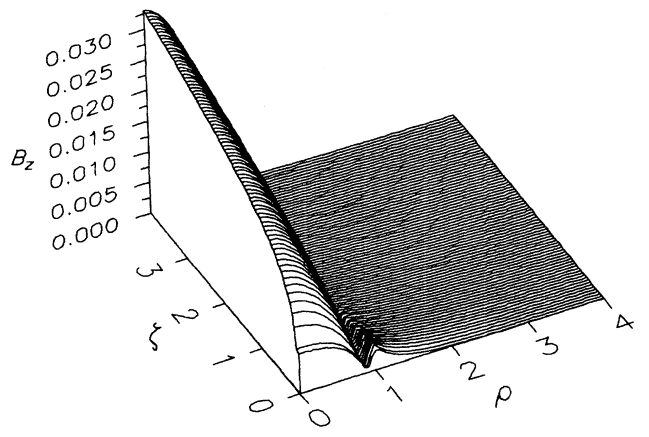

FIG. 13. Structure of the normalized $|B_z(\rho,\zeta)|$ wave-field component at $\sigma=0.05$ and $\Omega=0.6$ (weak magnetic field) in free fall or diffusion gas-discharge conditions ($\beta=0$).

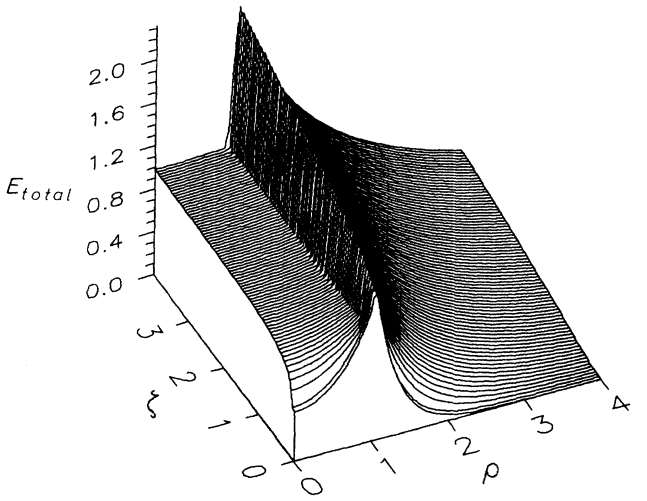

FIG. 15. Structure of the normalized $|E_{\text{total}}(\rho,\zeta)|$ wave field at $\sigma=0.05$ and $\Omega=0.6$ (weak magnetic field) in free fall or diffusion gas-discharge conditions ($\beta=0$).

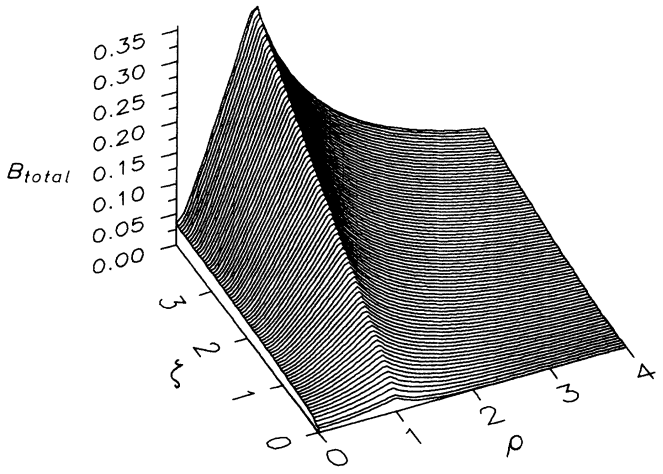

FIG. 16. Structure of the normalized $|B_{\text{total}}(\rho,\zeta)|$ wave field at $\sigma=0.05$ and $\Omega=0.6$ (weak magnetic field) in free fall or diffusion gas-discharge conditions ($\beta=0$).

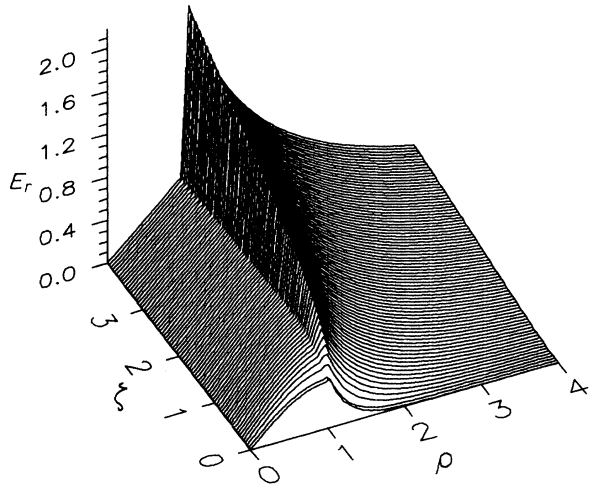

FIG. 18. Structure of the normalized $|E_r(\rho,\zeta)|$ wave-field component at $\sigma=0.2$ and $\Omega=2.5$ (strong magnetic field) in free fall or diffusion gas-discharge conditions ($\beta=0$).

experimental works [21,34] express their results in dimensional quantities. In order to compare the results, we need the values of two external parameters, namely ν and Q_β [cf. formulas (22)–(25)]. The magnitude of Q_β depends on the gas-discharge conditions. The available experimental data and theoretical results suggest that the gas-discharge regime is a diffusion one ($\beta=0$). In that case there exists a simple relation [30] between the mean power θ [8] required for maintaining an electron-ion pair in the discharge, and Q_0:

$$\theta=Q_0/\pi R^2 n_{cr}=(4e^2/m\omega^2R^2)Q_0 \ .$$

Thus the relations between the dimensionless and dimensional electron number density, axial coordinate, wave-field components, and wave power are as follows:

$$N=n/n_{cr}, \quad \zeta=\nu z/\omega R \ ,$$

$$E_{r,\varphi,z}=\mathcal{E}_{r,\varphi,z}/e_0 \ ,$$

$$B_{r,\varphi,z}=\mathcal{B}_{r,\varphi,z}/b_0 \ ,$$

$$S_*=S/s_0 \ ,$$

where

$$e_0(\mathrm{V\,cm^{-1}})=212(\omega/2\pi)(\mathrm{GHz})[(\theta/\nu)(\mathrm{eV})]^{1/2} \ ,$$

$$b_0(\mu\mathrm{T})=70.68(\omega/2\pi)(\mathrm{GHz})[(\theta/\nu)(\mathrm{eV})]^{1/2} \ ,$$

$$s_0(\mathrm{W})=39.231[(\omega/2\pi)(\mathrm{GHz})R\,(\mathrm{cm})]^3(\theta/\nu)(\mathrm{eV}) \ .$$

It is obvious that the values of the two external parameters ν and θ (respectively Q_0) become very important in the case of comparing our theoretical curves with dimensional ones.

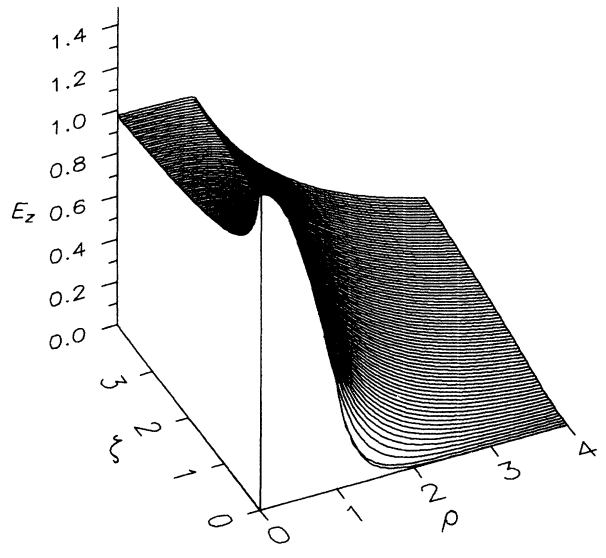

FIG. 17. Structure of the normalized $E_z(\rho,\zeta)$ wave-field component at $\sigma=0.2$ and $\Omega=2.5$ (strong magnetic field) in free fall or diffusion gas-discharge conditions ($\beta=0$).

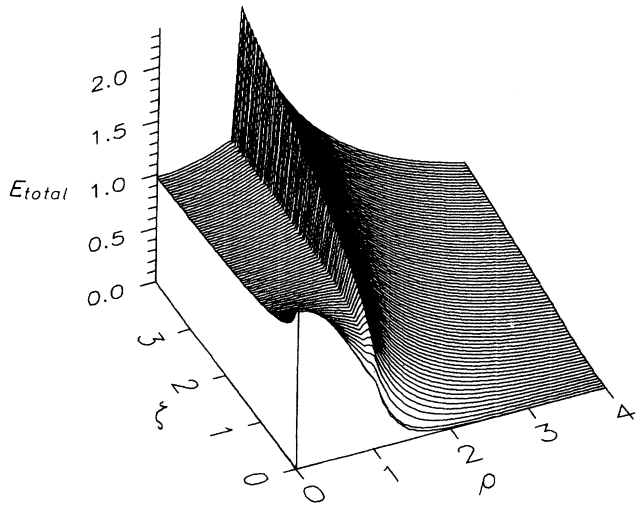

FIG. 19. Structure of the normalized $|E_{\text{total}}(\rho,\zeta)|$ wave field at $\sigma=0.2$ and $\Omega=2.5$ (strong magnetic field) in free fall or diffusion gas-discharge conditions ($\beta=0$).

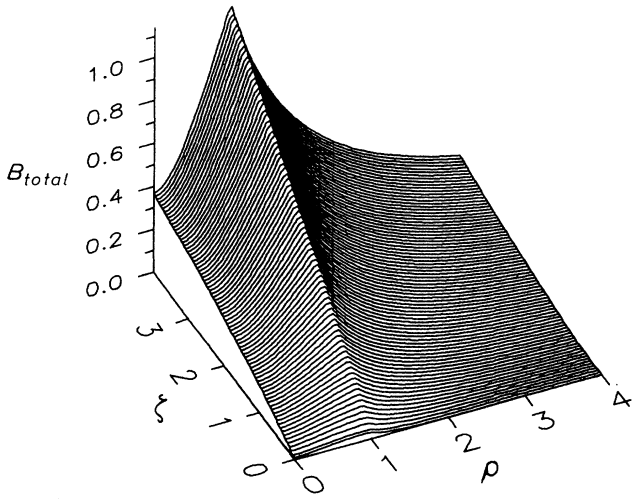

FIG. 20. Structure of the normalized $|B_{\text{total}}(\rho,\zeta)|$ wave field at $\sigma=0.2$ and $\Omega=2.5$ (strong magnetic field) in free fall or diffusion gas-discharge conditions ($\beta=0$).

Figure 21 shows the theoretical dimensionless plasma density axial profiles for the experimental conditions according to Fig. 16 in Ref. [34]: an argon plasma column at a pressure of 30 mTorr with a radius $R=0.75$ cm, wave frequency $\omega/2\pi=390$ MHz ($\sigma=0.0613$, respectively), at external magnetic fields of 100 and 455 G ($\Omega=0.7182$ and 3.268 correspondingly). The dotted line gives the electrostatic limit $\sigma=0$—one sees that for the given experimental situation, the electrostatic treatment is still adequate. In the same figure the experimental data are presented for convenience in dimensionless quantities.

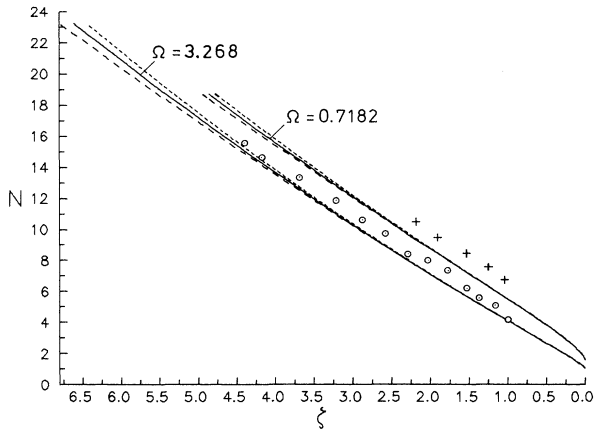

FIG. 21. Theoretical axial profiles (solid curves) of the normalized plasma density of two argon columns at pressure $p=30$ mTorr, $R=0.75$ cm, $\omega/2\pi=390$ MHz ($\sigma=0.0613$) in the presence of weak ($B_0=100$ G, $\Omega=0.7182$) and strong ($B_0=455$ G, $\Omega=3.268$) magnetic fields with electron concentrations near the exciter $n_{100\text{ G}}=3.5\times10^{10}$ cm^{-3} and $n_{455\text{ G}}=4.3\times10^{10}$ cm^{-3}, respectively. The experimental points have been taken from Fig. 16 of Pasquiers *et al.* [J. Appl. Phys. **65**, 1465 (1989)] with $\nu_{100\text{ G}}=1.56\times10^{8}$ s^{-1} and $\nu_{455\text{ G}}=1.19\times10^{8}$ s^{-1} correspondingly. The dashed curve illustrates the influence of the metal screen ($R_1=7.5$ cm, $\eta=10$), and the dotted one represents the electrostatic limit ($\sigma=0$) in the absence of a metal tube.

In order to do this we have used the values $\nu_{100\text{ G}}=1.56\times10^{8}$ s^{-1} and $\nu_{455\text{ G}}=1.19\times10^{8}$ s^{-1}, taken from theoretical curves, computed by Sá [37] and from Fig. 20 of Ref. [34]. We note that these collision frequencies are different from those in Fig. 16 of Ref. [34]—the latter are obtained by the method of best fit of the experimental and theoretical plasma density profiles. One sees from Fig. 21 that the experimental points are close to the theoretical curves but lie higher. The reason is that our model does not take into account the influence of the glass tube. Since in that case the metal screen is far enough from the discharge tube (the parameter $\eta=10$, dashed lines), its presence does not change the course of the axial profiles [31]. From our curves we obtain for the column lengths $z_{100\text{ G}}=57.1$ cm and $z_{455\text{ G}}=94.2$ cm, which is in agreement with the corresponding values in Fig. 16 of Ref. [34].

Figure 22 gives the axial profiles of the dimensionless wave power for the same experimental conditions as before. From these curves one can calculate the wave power necessary to sustain a plasma column with given length. For that reason we need the corresponding magnitudes of the parameter θ. The values of θ, calculated from Figs. 4 and 5 of Ref. [21], are $\theta_{100\text{ G}}=2.18\times10^{7}$ eV s^{-1} and $\theta_{455\text{ G}}=9.36\times10^{6}$ eV s^{-1}, respectively, which immediately give $S_{100\text{ G}}=6.8$ W and $S_{455\text{ G}}=5.9$ W. The corresponding experimental data are 7.5 and 5.4 W. These discrepancies are probably due to the neglecting of the dielectric tube in our model.

Pasquiers *et al.* [34] discuss the radial distribution of the wave electric field—in Fig. 4 (Ref. [34]) they present the radial profiles of the longitudinal and transverse electric field components as well as those of the total wave electric field calculated for different plasma densities and external magnetic fields. The behavior of these fields is similar to that presented in Figs. 11, 12, and 15 and 17–19. Figure 4(b) gives the radial structure of the wave electric field at the end of the column for a weak magnetic field ($\Omega=0.7182$) where the wave is a pure surface

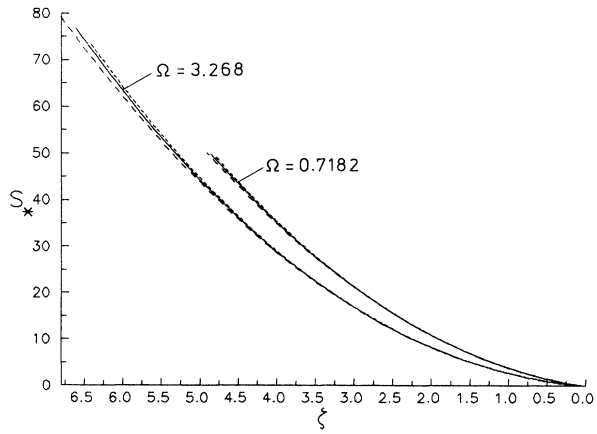

FIG. 22. Theoretical axial profiles of the normalized wave power of an azimuthally symmetric electromagnetic wave sustaining argon plasma columns at the same conditions as in Fig. 21.

mode (see Figs. 11 and 15). Figure 4(c) gives the radial structure of the wave electric field at a strong magnetic field ($\Omega=4$) near the wave exciter where the wave is a generalized surface mode (see Figs. 17 and 19), classified, however, by Pasquiers *et al.* as a surface wave. Figure 4(d) illustrates the case of a pseudosurface mode (strong magnetic field, end of the column), termed by the authors a volume wave. For long columns (large N) near the wave exciter, the wave is a generalized surface mode both for weak and strong magnetic fields (see Figs. 15 and 19). Such a situation is presented in Fig. 4(a), where the wave is called a surface wave. In the case of a strong magnetic field the $\mathcal{E}_r$ wave component is, however, much larger than that for a weak magnetic field. At strong magnetic fields, the $\mathcal{E}_z$ and $\mathcal{E}_r$ components are of the same order—so Fig. 4(a) is relevant only for weak magnetic fields.

VI. CONCLUSIONS

In this paper, we have presented a model of a low-pressure plasma column sustained by a traveling electromagnetic wave in the presence of an external axial magnetic field. The axial and radial structures of the wave-field components as well as the axial profiles of the wave number, wave power, and plasma column density have been obtained in suitable dimensionless quantities. This allows, for a given product wave frequency-plasma radius ωR at a fixed external magnetic field, the measurements for different gas pressures to be presented by one theoretical N-ξ (or S_*-ζ) curve, i.e., the model might be considered as a general one. We emphasize also that the model is applicable for each gas irrespective of its nature.

We have studied the influence of the parameters $\Omega=\omega_c/\omega$ and $\sigma=\omega R/c$ on the axial profiles of the wave-field components, wave number, wave power, and plasma column density for two gas-discharge regimes—free fall or diffusion ($\beta=0$) and recombination ($\beta=1$) ones. The results obtained show that only strong enough magnetic fields ($\Omega\geq 2.5$) change significantly the plasma column and electromagnetic wave parameters. The case of a weak magnetic field ($\Omega<1$) does not represent any practical interest. This model is not applicable as the wave frequency ω tends to the electron cyclotron frequency ω_c ($\Omega=1$).

The external magnetic field decreases the axial plasma density gradient and increases the column length for a fixed electron number density and/or wave power near the wave exciter—the stronger the magnetic field, the longer the column length. The magnetic field also changes the structure of the electromagnetic wave. Due to the plasma anisotropy, the wave is neither a TM nor a TE mode—it possesses all six components. Nevertheless, the $\mathcal{E}_z$ component is larger than the $\mathcal{B}_z$ one, so the wave should be classified as an EH wave. We emphasize that it is not a pure surface mode—almost everywhere the wave is a generalized surface mode, becoming at the column end a pure surface wave (for weak magnetic fields, $\Omega<1$) or a pseudosurface one (for strong magnetic fields, $\Omega>1$).

This model shows that the electrodynamical treatment is necessary for those experimental setups for which the magnitude of the parameter $\sigma=\omega R/c$ is large enough. For small σ's (say, $\sigma<0.1$), however, the simplest electrostatic model [32] might be used. We note also that the influence of σ on the plasma column parameters is similar to that for an isotropic plasma [28].

The agreement between our model and the available experimental data is acceptable. Obviously, for a more adequate and self-contained description, the model should include the presence of a dielectric container and a correct theoretical calculation of the collision frequency for momentum transfer ν and the mean power θ required for maintaining an electron-ion pair in the discharge.

ACKNOWLEDGMENTS

The authors would like to thank Ivan Ghanashev, Mladen Matev, Plamen Dankov, and Yurii Vorotnitsky for help in the programming. This work was supported in part by the Bulgarian Ministry of Science and Higher Education under Grant No. 443/87 and the Austrian Ministry of Science in the framework of Project 3.05 for scientific collaboration between Bulgaria and Austria.

*Also at Department of Physics, Institute for Foreign Students, BG-1111 Sofia, Bulgaria.

[1] J. Musil, Vacuum **36**, 161 (1986).
[2] M. Chaker, M. Moisan, and Z. Zakrzewski, Plasma Chem. Plasma Process. **6**, 79 (1986).
[3] M. Selby and G. M. Hieftje, Spectrochim. Acta B **42**, 285 (1987).
[4] M. Moisan and Z. Zakrzewski, in *Radiation Processes in Discharge Plasmas,* edited by J. Proud and L. H. Luessen (Plenum, New York, 1987), p. 381.
[5] V. M. M. Glaude, M. Moisan, R. Pantel, P. Leprince, and J. Marec, J. Appl. Phys. **51**, 5693 (1980).
[6] P. Leprince and J. Marec, J. Phys. **42**, 1421 (1981).
[7] M. Chaker and M. Moisan, J. Appl. Phys. **57**, 91 (1985).
[8] C. Boisse-Laporte, A. Granier, E. Dervisevich, P. Leprince, and J. Marec, J. Phys. D **20**, 197 (1987).
[9] K. Ivanova, I. Koleva, A. Shivarova, and E. Tatarova, in *Proceedings of the 19th ICPIG (Belgrade), 1989, Contributed Papers 2,* edited by J. M. Labat (University of Belgrade, Belgrade, 1989), p. 434.
[10] G. S. Solntsev, P. S. Boulkin, M. M. Rakhman, and L. I. Tsvetkova, Fiz. Plazmy **15**, 855 (1989).
[11] A. Granier, C. Boisse-Laporte, P. Leprince, J. Marec, and P. Nghiem, J. Phys. D **20**, 204 (1987).
[12] C. Boisse-Laporte, A. Granier, E. Bloyet, P. Leprince, and J. Marec, J. Appl. Phys. **61**, 1740 (1987).
[13] R. Darchicourt, S. Pasquiers, C. Boisse-Laporte, P. Leprince, and J. Marec, J. Phys. D **21**, 293 (1988).
[14] M. Moisan, Z. Zakrzewski, and R. Pantel, J. Phys. D **12**, 219 (1979).

[15] M. Moisan, Z. Zakrzewski, R. Pantel, and P. Leprince, IEEE Trans. Plasma Sci. **PS-12**, 203 (1984).
[16] M. Moisan, M. Chaker, Z. Zakrzewski, and J. Paraszczak, J. Phys. E **20**, 1356 (1987).
[17] M. Moisan and Z. Zakrzewski, Rev. Sci. Instrum. **58**, 1895 (1987).
[18] M. Moisan, P. Leprince, C. Beaudry, and E. Bloyet (unpublished).
[19] M. Moisan, R. Pantel, and A. Ricard, Can. J. Phys. **60**, 379 (1982).
[20] S. Pasquiers, A. B. Sa, and E. Bloyet, in *Proceedings of the 18th ICPIG (Swansea), 1987, Contributed Papers,* edited by W. Terry Williams (Hilger, Bristol, 1987), p. 846.
[21] S. Pasquiers, A. Granier, P. Leprince, and J. Marec, Europhys. Lett. **6**, 413 (1988).
[22] R. Anghelova, E. Benova, I. Koleva, P. Staikov, T. Stoychev, and I. Zhelyazkov, J. Phys. D **21**, 1371 (1988).
[23] E. Mateev, I. Zhelyazkov, and V. Atanassov, J. Appl. Phys. **54**, 3049 (1983).
[24] Z. Zakrzewski, J. Phys. D **16**, 171 (1983).
[25] C. M. Ferreira, J. Phys. D **16**, 1673 (1983).
[26] C. M. Ferreira, J. Phys. D **22**, 705 (1989).
[27] I. Zhelyazkov, E. Benova, and V. Atanassov, J. Appl. Phys. **59**, 1462 (1986).
[28] I. Zhelyazkov, V. Atanassov, and E. Benova, in *Surface Waves in Plasmas and Solids,* edited by S. Vuković (World Scientific, Singapore, 1986), p. 467.
[29] A. B. Sá and C. M. Ferreira, in *Europhysics Conference Abstracts ESCAMPIG 88,* edited by C. M. Ferreira and J. Heijn (European Physical Society, Geneva, 1988), Vol. 12H, p. 189.
[30] I. Zhelyazkov and E. Benova, J. Appl. Phys. **66**, 1641 (1989).
[31] E. Benova and I. Zhelyazkov, Phys. Scr. **43**, 68 (1991).
[32] I. Zhelyazkov, E. Benova, and V. Atanassov, J. Appl. Phys. **62**, 2713 (1987).
[33] T. C. Lim and G. W. Farnell, J. Appl. Phys. **39**, 4319 (1968).
[34] S. Pasquiers, C. Boisse-Laporte, A. Granier, E. Bloyet, P. Leprince, and J. Marec, J. Appl. Phys. **65**, 1465 (1989).
[35] Yu. M. Aliev, A. G. Boev, and A. P. Shivarova, Phys. Lett. **92A**, 235 (1982).
[36] S. T. Ivanov, E. G. Alexov, and P. N. Malinov, Plasma Phys. Control. Fusion **31**, 941 (1989).
[37] A. B. Sá, Ph.D. thesis, Lisbon Technical University, 1989.